



Contents lists available at ScienceDirect

Ceramics International

journal homepage: www.elsevier.com/locate/ceramint

Structure, mechanical properties and thermal stability of $Ti_{1-x}Si_xN$ coatings

Fei Pei^{a,b}, Yu X. Xu^{a,c}, Li Chen^{a,*}, Yong Du^a, Hou K. Zou^a

^a State Key Laboratory of Powder Metallurgy, Central South University, Changsha, Hunan 410083, China

^b Zhuzhou Cemented Carbide Cutting Tools Co., LTD, Zhuzhou, Hunan 412007, China

^c School of Electromechanical Engineering, Guangdong University of Technology, Guangzhou 510006, China

ARTICLE INFO

Keywords:

$Ti_{1-x}Si_xN$ coatings
Nanocomposite structure
Hardness
Thermal stability

ABSTRACT

$Ti_{1-x}Si_xN$ coating is a promising candidate for wear resistant applications due to their super-hardness and high thermal stability. Here, we explored the structure, mechanical properties and thermal stability of $Ti_{1-x}Si_xN$ ($x = 0, 0.13, 0.17$ and 0.22) coatings deposited by cathodic arc evaporation. Monolithically grown Si-containing $Ti_{1-x}Si_xN$ coatings, which are Si-solution in TiN for $x = 0.13$ and 0.17 , reveal a high hardness of 39.4 ± 0.67 and 40.6 ± 0.72 GPa, respectively. Then $Ti_{1-x}Si_xN$ transforms into a nanocomposite structure consisting of cubic Ti (Si)N nanocrystallite enveloped by the amorphous SiN_x tissue phase for $x = 0.22$, which exhibits a high hardness of 40.0 ± 0.6 GPa. However, increasing of Si content leads to a significant increase in compressive stress from -0.63 GPa for $x = 0$ to -3.78 GPa for $x = 0.13$ to -4.54 GPa for $x = 0.17$ to -5.51 GPa for $x = 0.22$. The hardness of $Ti_{1-x}Si_xN$ coatings can be maintained up to ~ 1000 °C due to the suppressed grain growth, and then decreases for further elevated annealing temperature, whereas the TiN coating exhibits a continuous drop in hardness towards its intrinsic value of ~ 21.3 GPa.

1. Introduction

TiN based protective coatings are widely used for wear resistant applications such as automotive and aerospace industries as well as cutting tools due to their high mechanical and thermal properties. Alloying with the third constituent elements (e.g., Al, Cr, Si) is a very effective method to tailor the structure and properties of TiN coatings [1–3]. Among them, $Ti_{1-x}Si_xN$ coatings, which were firstly invented by Li et al. [4], have been successfully applied in advanced machining technologies (e.g., high-speed and dry cutting) due to their super-hardness and high thermal stability. Veprek et al. [5–7] provided a network model with TiN nanograins (nc) encapsulated by amorphous (a) Si_3N_4 tissue phase (nc-TiN/a- Si_3N_4) to interpret the superhardness of $Ti_{1-x}Si_xN$. The super-hardness of nc-TiN/a- Si_3N_4 coatings, where the maximum hardness is obtained for Si content of 8–12 at% corresponding to a Si_3N_4 tissue phase with thickness of 1–2 monolayers [8–12], can be related to two primary reasons: 1) nucleation and glide of dislocations are prevented within the small dimensions across the TiN nanograins; 2) a well-defined interface of high cohesive strength inhibits grain-boundary sliding [12,13]. Additionally, the nc-TiN/a- Si_3N_4 coating exhibits high thermal stability with an almost invariable hardness after annealing up to 1100 °C, due to the retarded coarsening of TiN grains by the Si_3N_4 tissue phase [8,9]. However, the structure of $Ti_{1-x}Si_xN$ coatings is far more complicated than the nc-TiN/a- Si_3N_4

model. Si substitutionally incorporated on Ti sites in TiN is also observed in many reports [13–17]. The single-phase cubic $Ti_{1-x}Si_xN$ coatings via epitaxial growth on TiN(111)/MgO(111) reveal a high solubility of $x = 0.19$ [16]. Up to now the reported maximum solubility limitation of Si in TiN is 24 at% (namely $Ti_{0.76}Si_{0.24}N$), which is deposited using hybrid high-power pulsed and dc magnetron co-sputtering [17]. Furthermore, Flink et al. [18] reported a structural transformation of $Ti_{1-x}Si_xN$ coatings from Si substitutionally solutions on Ti sites in TiN for $x \leq 0.09$ to a mixed structure consisting of cubic TiSiN nanocrystallite fibrous bundles separated by metastable SiN_x with coherent-to-semicoherent interfaces for $x > 0.09$. Meanwhile, the high hardness of $Ti_{1-x}Si_xN$ coatings for $0.04 \leq x \leq 0.20$ is retained after annealing to 1000 °C due to the Si segregation to form the strong coherent crystalline SiN_x phase, which hinders further recrystallization and strain relaxation [18,19]. Evidencing the high hardness up to ~ 40 GPa as well as good thermal stability, the $Ti_{1-x}Si_xN$ coatings are promising candidates for industrial applications.

However, a detailed study on the structure and thermal stability of $Ti_{1-x}Si_xN$ coatings has not yet been explored. In this work, we researched the structure, mechanical properties and thermal stability of $Ti_{1-x}Si_xN$ ($x = 0, 0.13, 0.17$ and 0.22) coatings. Especially, the structural evolution of $Ti_{1-x}Si_xN$ coating during thermal exposure and corresponding hardness variation were investigated in detail.

* Corresponding author.

E-mail address: chenli_927@126.com (L. Chen).

<https://doi.org/10.1016/j.ceramint.2018.05.210>

Received 27 April 2018; Received in revised form 23 May 2018; Accepted 24 May 2018
0272-8842/ © 2018 Published by Elsevier Ltd.

2. Experimental details

Ti_{1-x}Si_xN coatings were deposited on Si(100) wafers (20 × 7 × 0.4 mm³, both side polished), low-alloy steel foils (200 × 150 × 0.05 mm³), mirror polished tungsten (W) plates (10 × 10 × 3 mm³) using an industrial-scaled cathodic arc evaporation system (Balzers Oerlikon Rapid Coating System, RCS) equipped with Ti_{1-x}Si_x (x = 0, 0.15, 0.20 and 0.25) targets. Different substrates were used for the individual investigations: Si(100) for residual stress tests; low-alloy steel foils for X-ray diffraction tests of as-deposited and annealed coatings and W plates for hardness tests of as-deposited and annealed samples. Prior to the depositions, the used substrates were ultrasonically cleaned in acetone and ethanol, as well as thermally cleaned for 30 min at 550 °C with Ar ion etched within the chamber. The deposition process for all coating is performed in pure nitrogen pressure of ~ 3.2 Pa, 550 °C, 150 A for target current and -40 V for DC bias.

Freestanding coating powder, which is obtained by grinding the coating after chemical etching from low-alloy steel foil substrates in 10 mol% nitric acid in order to eliminate substrate interference, was annealed in a differential scanning calorimetry machine (Netzsch-STA 409C, Germany) from room temperature to target temperatures (T_a) of 800, 900, 1000, 1100, 1200, 1300, 1450 and 1550 °C with a heating rate of 10 K/min and then cool down immediately with a cooling rate of 50 K/min in flowing Ar (99.9% purity, 20 sccm flow rate). Vacuum annealing of our coatings on W plates was conducted in a vacuum furnace (COD533R, pressure ≤ 0.1 mPa) to T_a = 800, 900, 1000, 1100, and 1200 °C with a heating rate of 10 K/min, holding period of 30 min at peak temperature and then oven-cooling to room temperature.

Chemical composition analysis of the Ti_{1-x}Si_xN coatings was determined using electron probe microanalysis (EPMA) (JXA-8800R, JEOL). Quantification of the elements was obtained by elemental standards and a TiN coating standard which has been quantified by Rutherford Backscattering Spectroscopy. X-ray diffraction (XRD) analyses of as-deposited and annealed free-standing coating powder were performed using a Bruker D8 diffractometer in Bragg/Brentano mode at 40 mA and 40 kV. Detailed characterizations of our as-deposited and annealed coatings were performed by transmission electron microscopy (TEM) and scanning transmission electron microscopy (STEM) observations using an FEI Titan G2 60-300 operated at 300 kV. TEM specimens were prepared using a dual-beam focused ion beam (FIB) system (FEI Helios Nanolab 600i) following the lift-out procedure. Final surface cleaning was conducted at 5 kV and 41 pA to minimize Ga ion implantation and artifacts. Residual stresses, σ , of our coatings were determined by biaxial residual stress measurements using the substrate curvature method. Detailed information on the measurement and calculation of σ is described in Ref. [20]. The coating thickness on Si(100) substrates for stress measurements was kept constant at ~ 1.0 μ m, and the coating thickness on W pieces for hardness measurements was kept constant at ~ 2.5 μ m. The hardness and elastic modulus of as-deposited and annealed coatings on W plates were measured by an instrumented nanoindentation equipped with a Berkovich tip (CSM Instruments, Switzerland), and then calculated from the load-displacement curves according to the Oliver and Pharr method [21]. According to the experimental results based on the large-load (30 mN) penetration test, a smaller penetration load of 15 mN was chosen to measure the mechanical properties of the coatings to keep the indentation depth of ~ 160 nm, which is below 10% of the coating thickness.

3. Results and discussion

3.1. Structure and morphology

When normalizing the (Ti + Si)/nitrogen atomic ratio to 1:1, the chemical compositions of Ti_{1-x}Si_xN monolithic coatings obtained by EPMA are TiN, Ti_{0.87}Si_{0.13}N, Ti_{0.83}Si_{0.17}N and Ti_{0.78}Si_{0.22}N corresponding to the used targets of Ti, Ti_{0.85}Si_{0.15}, Ti_{0.80}Si_{0.20}, and

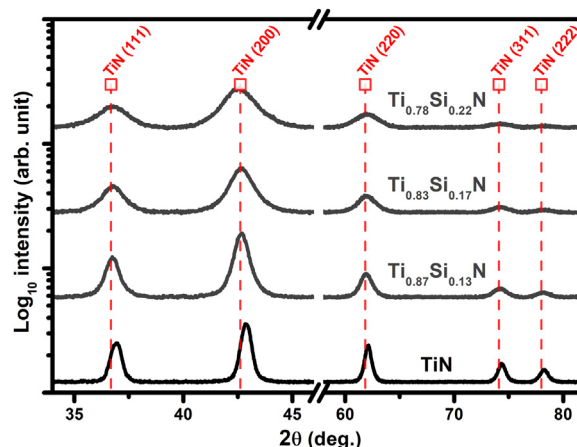


Fig. 1. XRD patterns of TiN and Ti_{1-x}Si_xN coating samples.

Ti_{0.75}Si_{0.25}, respectively. The Si content within the coatings is slightly lower than within the corresponding targets, which can be attributed to the combined effects such as resputtering, evaporation behavior of the target material, or gas phase scattering [22].

XRD results of Ti_{1-x}Si_xN coatings in Fig. 1 reveal a face-centered cubic (FCC) structure. No signals are observed for SiN_x or titanium silicide crystal, suggesting that Si-existence is either substitution solid solution of Si in TiN, or amorphous SiN_x accumulated at the TiN grain boundaries. Alloying with 13 at% Si into TiN causes a shift of diffraction peak positions to lower 2 θ angles, however, with increasing of Si content a reverse shift of the peak positions to higher 2 θ angles for Ti_{0.84}Si_{0.16}N and Ti_{0.78}Si_{0.22}N coatings is observed. This change is related to the variation of lattice parameters and/or stresses. As obtained by calculation from the XRD peak position and Rietveld analysis, the lattice parameters of Ti_{1-x}Si_xN coatings are 4.239 Å for x = 0, to 4.242 Å for x = 0.13, to 4.239 Å for x = 0.16, 4.236 Å for x = 0.22, respectively. Additionally, alloying with Si into TiN causes a significant broadening of XRD peaks due to grain refinement and/or increased microstrains.

Cross-sectional TEM and high-resolution transmission electron microscopy (HRTEM) investigations of the Ti_{1-x}Si_xN coatings were performed in order to further study their microstructure. Fig. 2 shows TEM bright-field (BF) images of Ti_{1-x}Si_xN coatings, together with corresponding selected area electron diffraction (SAED) patterns and lattice resolved HRTEM as well as fast Fourier transformation (FFT) and inverse fast Fourier transformation (IFFT) images. TEM-BF image of Fig. 2a indicates a dense columnar structure with grains elongated in the growth direction, and the width of columnar grains is 10–50 nm. The diffraction arcs and rings of SAED pattern (Fig. 2a insert) corresponding to the polycrystalline columnar structure indicate that the Ti_{0.87}Si_{0.13}N coating is a single-phase cubic structure. This is in good agreement with the previous XRD investigations (Fig. 1). HRTEM analysis of the grain boundaries was conducted to determine if there is SiN_x tissue among nano-columnar grains. HRTEM image in Fig. 2b shows the grain boundary of two adjacent columnar grains exhibiting [001] zone axis only with a small orientation difference. This can be better seen by the IFFT image of a square region outlined by the box in Fig. 2c. The FFT spots of Fig. 2c are a bit elliptical due to the overlapping of two sets of FCC reflexes. Based on the above investigations, an encapsulating amorphous or polycrystalline SiN_x tissue phase among grains as reported for the columnar structure in Ref. [18] is not observed. Additionally, the EDS mapping (not shown here) does not find Si segregation in the grain boundaries. Therefore, the present results indicate that Si in Ti_{0.87}Si_{0.13}N is substitutionally incorporated on Ti sites in TiN.

With increasing x to 0.17, the columnar grain structure disappears. The pronounced grain refinement causes a relatively equiaxed

Download English Version:

<https://daneshyari.com/en/article/7886360>

Download Persian Version:

<https://daneshyari.com/article/7886360>

[Daneshyari.com](https://daneshyari.com)